

EFFICIENT COSMIC RAY ACCELERATION, HYDRODYNAMICS, AND SELF-CONSISTENT THERMAL X-RAY EMISSION APPLIED TO SNR RX J1713.7-3946

DONALD C. ELLISON,¹ DANIEL J. PATNAUDE,² PATRICK SLANE,² AND JOHN RAYMOND²*Draft version May 2, 2019*

ABSTRACT

We model the broad-band emission from SNR RX J1713.7-3946 including, for the first time, a consistent calculation of thermal X-ray emission together with non-thermal emission in a nonlinear diffusive shock acceleration (DSA) model. Our model tracks the evolution of the SNR including the plasma ionization state between the forward shock and the contact discontinuity. We use a plasma emissivity code to predict the thermal X-ray emission spectrum assuming the initially cold electrons are heated either by Coulomb collisions with the shock heated protons (the slowest possible heating), or come into instant equilibration with the protons. For either electron heating model, electrons reach $\gtrsim 10^7$ K rapidly and the X-ray line emission near 1 keV is more than 10 times as luminous as the underlying thermal bremsstrahlung continuum. Since recent *Suzaku* observations show no detectable line emission, this places strong constraints on the unshocked ambient medium density and on the relativistic electron to proton ratio. For the uniform circumstellar medium (CSM) models we consider, the low densities and high relativistic electron to proton ratios required to match the *Suzaku* X-ray observations *definitively rule out pion-decay* as the emission process producing GeV-TeV photons. We show that leptonic models, where inverse-Compton scattering against the cosmic background radiation dominates the GeV-TeV emission, can produce satisfactory fits to the broad-band thermal and non-thermal observations in a uniform CSM.

Subject headings: acceleration of particles, shock waves, ISM: cosmic rays, ISM: supernova remnants, magnetic fields, turbulence

1. INTRODUCTION

The supernova remnant RX J1713.7-3946 (G347.3-0.5) has been detected at photon energies ranging from radio to TeV γ -rays. The GeV-TeV detections in particular make this SNR an important test-bed for models of particle acceleration in astrophysical shocks, and a large number of fits to the data have been presented with an array of environmental and particle acceleration parameters. Invariably, parameters are found that allow good fits to the non-thermal observations (or some sub-set of the observations). A critical question for cosmic-ray (CR) origin concerns the production of the GeV-TeV γ -rays. Are these γ -rays primarily from inverse-Compton (IC) emission from relativistic electrons, or pion-decay emission from the interaction of relativistic hadrons with the ambient medium? Models with good fits to the TeV emission with either inverse-Compton or pion-decay have been presented (e.g., Porter, Moskalenko & Strong 2006; Berezhko & Völk 2008; Tanaka et al. 2008; Morlino, Amato & Blasi 2009; Zirakashvili & Aharonian 2009). One way to discriminate between IC and pion-decay models is to examine the thermal X-ray emission, because the pion-decay models require a high proton number density, n_p , and the thermal emission scales as n_p^2 .

Until now however, fits to the broad-band emission that incorporate nonlinear diffusive shock acceleration (DSA) have not accurately accounted for the thermal X-

ray emission that might be present. We do this here for a SNR evolving in a uniform circumstellar medium (CSM) with no density enhancements as might occur with a pre-SN dense shell, nearby molecular cloud, etc. We find that the lack of observed thermal line emission *eliminates pion-decay* as the source of TeV emission in models with uniform circumstellar media.

The essential elements of our CR-hydro-NEI model have been presented in Ellison & Cassam-Chenaï (2005); Ellison et al. (2007); Patnaude, Ellison & Slane (2009), and references therein. We couple a one-dimensional hydrodynamic simulation of an evolving SNR with nonlinear diffusive shock acceleration. The ionization structure, free electron number density, and electron temperature in the evolving interaction region between the forward shock (FS) and contact discontinuity (CD) are determined with a self-consistent treatment of the nonequilibrium ionization (NEI). We couple our computed nonequilibrium ionization fractions of heavy elements to an updated version of the Raymond & Smith (1977) plasma emissivity code to compute the thermal X-ray emission.

Simultaneously, the shock accelerated, non-thermal electron and proton spectra are calculated, evolved, and used to determine the synchrotron, IC, non-thermal bremsstrahlung, and pion-decay emission from the SNR. We therefore obtain, for the first time, consistent thermal and non-thermal emission in an evolving SNR.

2. MODEL

Any reasonably complete broad-band model of a SNR has a host of parameters. SNR RX J1713.7-3946 is no exception and in this paper we do not present a full parameter search. Instead, we concentrate on three essen-

¹ Physics Department, North Carolina State University, Box 8202, Raleigh, NC 27695, U.S.A.; don_ellison@ncsu.edu, avladim@ncsu.edu

² Smithsonian Astrophysical Observatory, MS-3, 60 Garden Street, Cambridge, MA 02138, USA

tial coupled components: (1) the SNR hydrodynamics, (2) nonlinear DSA, and (3) non-equilibrium ionization.

Following the majority of work on SNR RX J1713.7-3946, we assume an age $t_{\text{SNR}} \simeq 1600$ yr, and a distance $D_{\text{SNR}} \simeq 1$ kpc. Using the observed angular size, D_{SNR} implies a forward shock radius $R_{\text{FS}} \simeq 8.7$ pc. While SNR RX J1713.7-3946 is believed to be a core-collapse SN, we again follow the majority of work on this remnant and assume a uniform CSM with constant proton number density, n_p , and constant unshocked magnetic field, B_0 . We will present models where a pre-SN wind is assumed in future work. Besides n_p and B_0 , the following environmental parameters are required to model the SNR evolution: the SN explosion energy, E_{SN} , the ejecta mass, M_{ej} (we assume an exponential mass distribution for the ejecta), and the temperature of the unshocked CSM, T_0 .

We show models with two sets of parameters. In the “hadronic” model, the parameters are such that the GeV-TeV emission is dominated by pion-decay, while in the “leptonic” model, IC produces the GeV-TeV emission. In both cases, the parameters are chosen to simultaneously match the HESS TeV observations (Aharonian et al. 2006) and the *Suzaku* X-ray continuum (Tanaka et al. 2008). The hadronic and leptonic names refer to the particles, protons or electrons, mainly responsible for the GeV-TeV emission. As we show below, both models place the majority of the accelerated particle energy in protons, not electrons.

We include an amplification factor, B_{amp} , for the shocked magnetic field. In our simple *ad hoc* model of magnetic field amplification (MFA), the compressed magnetic field immediately behind the shock is increased by a factor B_{amp} . The amplified downstream field is then evolved in the downstream region as described in Ellison et al. (2007). For more self-consistent models of MFA see, for example, Vladimirov, Ellison & Bykov (2006); Caprioli et al. (2008); Vladimirov, Bykov, & Ellison (2009).

To model the nonthermal radiation, we need additional parameters for nonlinear DSA.³ These are the acceleration efficiency, \mathcal{E}_{DSA} (i.e., the instantaneous fraction of shock ram kinetic energy flux placed in superthermal protons), the relativistic electron to relativistic proton ratio, K_{ep} ,⁴ the maximum energy the protons obtain E_p^{max} , and a factor, α_{cut} , characterizing the shape of the turnover region around E_p^{max} . We determine E_p^{max} by limiting the acceleration when the acceleration time matches the SNR age or when the upstream diffusion length matches some fraction, f_{sk} , of

³ The model of nonlinear DSA we use here is based on the semi-analytic model developed by Blasi, Gabici & Vannoni (2005) and Amato & Blasi (2006). In our implementation, we fix the acceleration efficiency rather than the injection fraction as is done by Blasi and co-workers. While this difference may have important consequences during the early stages of the SNR evolution when the FS Mach number is extremely large (see Berezhko & Ellison 1999), it makes no significant difference to the integrated spectra at the later times we show here.

⁴ Note that K_{ep} sets the post-shock relativistic electron density given the post-shock relativistic proton density. The post-shock thermal electron density, which determines the bremsstrahlung continuum and the X-ray line emission, is set by the densities and ionization states of the post-shock hydrogen and heavier elements. The model parameters K_{ep} and n_p are independent.

the shock radius, whichever comes first.⁵ The factor α_{cut} smoothes the particle spectrum around E_p^{max} mimicking the effects of particle escape. The above parameters are fully defined in Ellison, Decourchelle & Ballet (2004) and Ellison & Cassam-Chenaï (2005). The efficiency of DSA has been directly measured at the quasi-parallel Earth bow shock with $\mathcal{E}_{\text{DSA}} \gtrsim 0.25$ (Ellison, Moebius & Paschmann 1990). Indirect evidence, based on particular models, suggests that the efficiency in some young SNRs, at least in some regions of the FS, can be 50% or more (e.g., Völk, Berezhko & Ksenofontov 2003; Warren et al. 2005; Helder et al. 2009).

For the thermal X-ray emission, we assume cosmic abundances and compare two extremes for heating the initially cold electrons. The slowest possible heating is from Coulomb collisions and the fastest is instant equilibration between electrons and protons, presumably produced by wave-particle interactions. For shock speeds above ~ 1000 km s⁻¹, it has been suggested that electrons are heated very rapidly to $kT \sim 0.3$ keV by lower hybrid waves, after which continued heating to $kT \sim 1$ keV proceeds through Coulomb collisions (e.g., Ghavamian, Laming & Rakowski 2007). Since, as we show below, Coulomb collisions alone rapidly heat the gas to ~ 0.3 keV, any difference between lower hybrid wave heating and Coulomb heating would only be important for UV and optical lines, so pure Coulomb models are appropriate for the X-ray emission.

It is important to note that, in our CR-hydro-NEI model for the interaction region between the CD and FS, including X-ray line emission only requires two additional assumptions. One is the CSM elemental abundance and the other is the electron heating model. For Type Ia SNe, and a wide range of low-to-moderate mass core-collapse SNe, it is reasonable to assume solar abundances for the CSM (e.g., Chiosi & Maeder 1986; Kudritzki & Puls 2000). The two heating extremes we consider cover all likely possibilities.

3. RESULTS

For our leptonic model we assume $n_p = 0.05$ cm⁻³, $B_0 = 3$ μ G, $\mathcal{E}_{\text{DSA}} = 0.25$, $K_{\text{ep}} = 2 \times 10^{-2}$, $B_{\text{amp}} = 1$, $f_{\text{sk}} = 0.1$, and $\alpha_{\text{cut}} = 1$. For the hadronic model, $n_p = 0.2$ cm⁻³, $B_0 = 2$ μ G, $\mathcal{E}_{\text{DSA}} = 0.5$, $K_{\text{ep}} = 7 \times 10^{-4}$, $B_{\text{amp}} = 5$, $f_{\text{sk}} = 0.05$, and $\alpha_{\text{cut}} = 1$. In both models, the values for E_{SN} and M_{ej} are varied with n_p to obtain $R_{\text{FS}} \sim 8 - 10$ pc at $t_{\text{SNR}} = 1600$ yr. Thus, for the leptonic model, $E_{\text{SN}} = 1 \times 10^{51}$ erg and $M_{\text{ej}} = 3 M_{\odot}$, while the hadronic model uses $E_{\text{SN}} = 2 \times 10^{51}$ erg and $M_{\text{ej}} = 1.4 M_{\odot}$.⁶ For a particular n_p , other combinations of E_{SN} and M_{ej} giving $R_{\text{FS}} \simeq 8 - 10$ pc at 1600 yr yield similar results. In all cases, we assume $T_0 = 10^4$ K.⁷

At the end of the simulation, we obtain for the leptonic (hadronic) model: the forward shock radius $R_{\text{FS}} \simeq 9.3$ (8.8) pc; the forward shock speed $V_{\text{FS}} \simeq$

⁵ The diffusion length in the FS precursor is determined assuming “Bohm diffusion,” where a particle’s mean free path is on the order of its gyroradius.

⁶ The value $M_{\text{ej}} = 1.4 M_{\odot}$ is not meant to imply that we believe SNR RX J1713.7-3946 originated from a Type Ia supernova.

⁷ As long as $T_0 \lesssim 10^6$ K, the unshocked temperature only weakly influences our results.

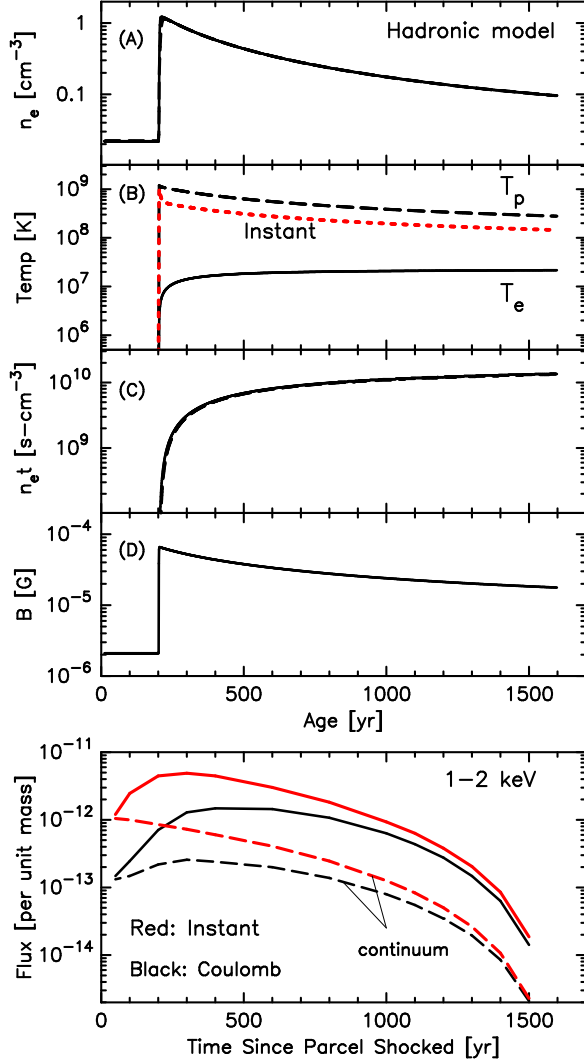


FIG. 1.— The top four panels show the free electron density, n_e , the temperature, the ionization age, $n_e t$, and the magnetic field in a parcel of gas first shocked at 200 yr. In panels (A) and (C), the solid curves are for Coulomb equilibration and the dashed curves (barely visible) are for instant equilibration. In panel (B), the dashed curve is the proton temperature and the solid curve the electron temperature assuming Coulomb equilibration. The dotted red curve in (B) shows the equal electron and proton temperatures assuming instant equilibration. In the bottom panel, the solid curves show the total emitted flux, at $t_{\text{SNR}} = 1600$ yr, per arbitrary unit mass, in the band 1–2 keV from parcels of gas shocked at previous times. The dashed curves in the bottom panel show the corresponding flux from the bremsstrahlung continuum. The parameters are for our hadronic model with $n_p = 0.2 \text{ cm}^{-3}$.

3000 (2300) km s⁻¹; the magnetic field immediately behind the FS $B_2 \simeq 10$ (36) μG ; the overall FS compression ratio $R_{\text{tot}} \simeq 4.6$ (5.6), the subshock compression ratio $R_{\text{sub}} \simeq 3.98$ (3.86), the fraction of SN explosion energy placed in CR ions $\simeq 0.13$ (0.4), and the mass swept up by the FS $\simeq 6$ (19) M_\odot .

In Fig. 1 we illustrate the properties of our CR-hydro-NEI model by following particular parcels of plasma. In the top four panels we show, for our hadronic model, the free electron number density, n_e , the electron and proton temperatures, the ionization parameter or age, $n_e t$ (t is the time since the parcel was shocked), and the magnetic field in a parcel of plasma that is overtaken by the FS at 200 yr. The red dotted curve in panel (B) gives the tem-

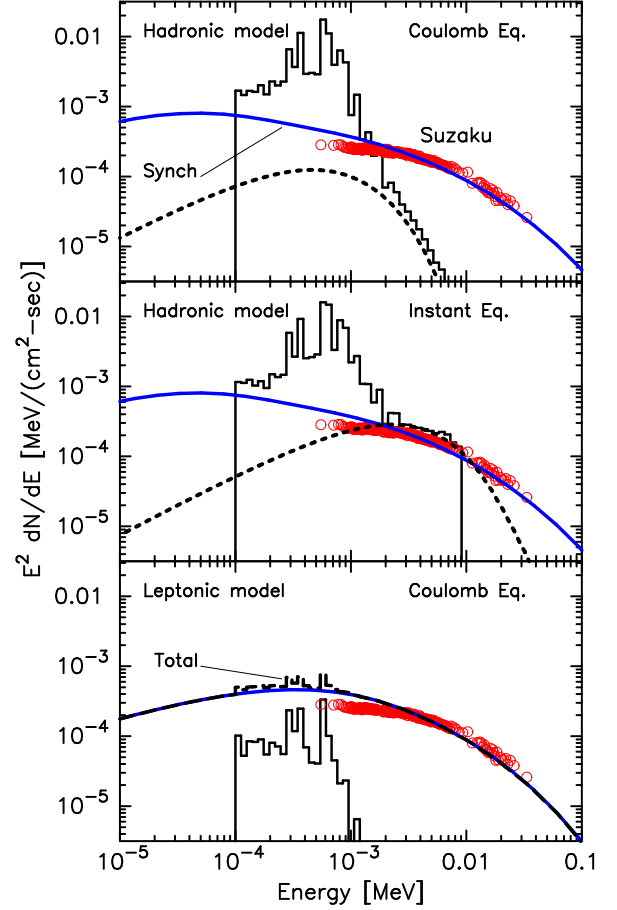


FIG. 2.— The top two panels show fits to the *Suzaku* RX J1713.7-3946 observations with our hadronic model for both Coulomb and instant temperature equilibration but ignoring the X-line emission. The blue solid curve is the synchrotron continuum, the black solid curve is the thermal emission (only lines above 10⁻⁴ MeV are included), and the dotted curve is the underlying bremsstrahlung continuum. The observed emission would be the sum (not shown in the top two panels) of the solid black and blue curves. The bottom panel shows the leptonic model (with Coulomb equilibration) where parameters have been chosen to be consistent with the *Suzaku* observations. For the hadronic model, the radiation intensity is multiplied by 0.95 to match the observations. For the leptonic model, a normalization factor of 0.2 is required to match the observations. We note that the *Suzaku* data have been adjusted for interstellar extinction so no extinction is applied to the model.

perature assuming instant equilibration. Even though $T_e/T_p \lesssim 0.1$ throughout the simulation for Coulomb equilibration, T_e approaches 10⁷ K (~ 850 eV) rapidly before leveling out.

In the bottom panel of Figure 1, we plot the thermal X-ray emission between 1 and 2 keV, for both instant and Coulomb equilibration, at the end of the simulation for parcels of plasma shocked at previous times. The dashed curves are the continuum emission between 1 and 2 keV and the total emission (solid curves), including lines, stands well above this regardless of the electron equilibration. As the left end of the bottom panel shows, at $t_{\text{SNR}} \simeq 1600$ yr, plasma that was shocked $\gtrsim 200$ years earlier is sufficiently ionized to produce a substantial flux in lines regardless of the electron equilibration.

In the top two panels of Figure 2 we compare our hadronic model to *Suzaku* observations of J1713 (Tanaka et al. 2008) for Coulomb (top panel) and in-

stant equilibration (middle panel). The *Suzaku* observations have been adjusted for interstellar extinction and all model parameters are the same as in Fig. 1. For our hadronic model, we have chosen parameters that result in pion-decay dominating the GeV-TeV emission, i.e., n_p must be above some limit and K_{ep} must be below some limit for this to be the case. Figure 2 makes it clear, however, that the X-ray line emission is much stronger in the hadronic model than can be accommodated by observations. The only way to lower this emission relative to the synchrotron continuum would be to increase K_{ep} or to decrease n_p to values that would then no longer reproduce the observed gamma-ray emission. This is true regardless of the electron equilibration. We note that lowering n_p in uniform CSM models requires lowering E_{SN} to maintain $R_{FS} \sim 8 - 10$ pc.

We are unable to find any set of parameters that gives pion-decay dominating the TeV emission without producing emission lines around 1 keV that are inconsistent with the *Suzaku* observations.

In the bottom panel of Figure 2 we show our leptonic model where we have chosen parameters to be consistent with the smooth *Suzaku* observations. In addition to the parameters discussed already, we have arbitrarily adjusted the overall normalization of both models to match the observations. The hadronic model has been multiplied by 0.95 and the leptonic model by 0.2. Normalization values < 1 might correspond, observationally, to a partially complete shell morphology for the SNR, or possibly some reduction in the DSA injection and/or acceleration efficiency over some fraction of the SNR surface (e.g., Berezhko & Völk 2008).

In Figure 3, we show our best fit hadronic and leptonic models, folded through the *Suzaku* XIS instrument response.⁸ For both models, we simulated 20 ks observations of the entire SNR with no background subtraction, assuming a Galactic column density $n_H = 7.9 \times 10^{21} \text{ cm}^{-2}$. When compared to the *Suzaku* observations (cf., Figs. 10 or 11 in Tanaka et al. 2008), it is clear that *Suzaku* would have detected lines as strong as those produced in our hadronic model had they been present.

In Fig. 4, we show broad-band fits to radio, *Suzaku*, preliminary *Fermi-LAT*, and HESS observations of RX J1713.7-3946. The hadronic and leptonic models both produce reasonable fits if the thermal X-ray emission is ignored. When the thermal X-rays are considered, the hadronic model is excluded. Only the cosmic microwave background is used to determine the IC emission.

It is important to note in considering Figs. 2 and 4 that equally good fits to the *continuum* observations can be obtained with different parameter combinations. This, and the fact that the various models that have been applied to RX J1713.7-3946 differ in details, accounts for the relatively small differences in parameters we obtain compared to those obtained by other modelers (e.g., Berezhko & Völk 2008; Morlino, Amato & Blasi 2009). However, consistency with the thermal X-ray line emission forces the CSM density down and K_{ep} up so no set of parameters can be found that result in pion-decay dominating the GeV-TeV emission.

Characteristic of efficient DSA, the CR-hydro-NEI

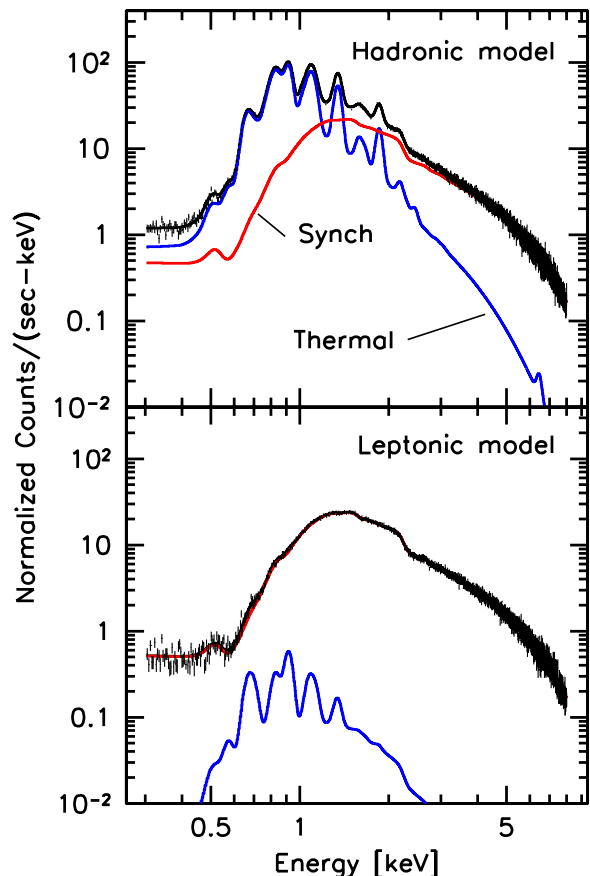


FIG. 3.— Simulated *Suzaku* XIS spectra of RX J1713.3-3946. In the top panel, the best fit hadronic model is shown, with $n_p = 0.2 \text{ cm}^{-3}$, while in the bottom panel, the best fit leptonic model is shown, with $n_p = 0.05 \text{ cm}^{-3}$. In both panels, the blue curve is the contribution from the thermal X-ray emission, while the red curve is the contribution from synchrotron emission. The spectra correspond to a simulated 20 ks observation and are normalized to match the unabsorbed 1.0 - 10.0 keV flux of $7.65 \times 10^{-10} \text{ erg cm}^{-2} \text{ s}^{-1}$ found by Tanaka et al. (2009). In these simulated observations, we assume a Galactic $n_H = 7.9 \times 10^{21} \text{ cm}^{-2}$.

model produces an overall shock compression, $R_{tot} > 4$, and a subshock compression, $R_{sub} < 4$. Nevertheless, even with 50% efficiency ($\mathcal{E}_{DSA} = 0.5$), R_{sub} remains large enough for electrons temperatures to be high enough for strong line production.

The only factor we see that could lower the thermal emission substantially in a uniform CSM model, is the abundance. If the CSM is nearly devoid of heavy elements, thermal line emission will be suppressed. Depletion onto dust will cut down C, Mg, Si and Fe, but it will not affect the O lines, which are the brightest in the model, or N or Ne. Furthermore, a substantial fraction of the dust is destroyed once n_{et} becomes a few times $10^{10} \text{ s-cm}^{-3}$, so some of the refractory elements would be liberated (e.g., Williams et al. 2006). One does not expect really severe depletion in the low density uniform medium, but there could be significant dust in a red giant wind.

It is also possible that the progenitor was a Wolf-Rayet (WR) star, and this could give anomalous abundances (e.g., Crowther 2007). Conversion of H to He reduces the number of electrons, weakening the line emission per unit mass by as much as a factor of two. However, WC

⁸ Response matrices are available at http://heasarc.nasa.gov/docs/suzaku/prop_tools/xis_mat.html.

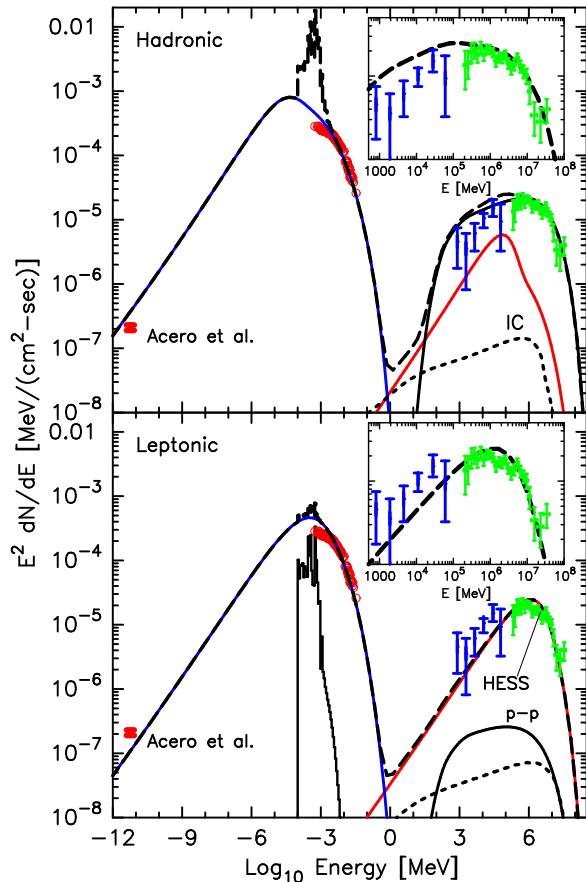


FIG. 4.— Broad-band fits to radio (Acero et al. 2009), *Suzaku* (Tanaka et al. 2008), preliminary *Fermi-LAT* (Funk et al. 2009), and HESS observations (Aharonian et al. 2006) of RX J1713.7-3946. The top panel is our hadronic model and the bottom panel is our leptonic model. In both cases, the blue curve is synchrotron, the black is pion-decay, the red is IC, and the dotted is non-thermal bremsstrahlung. The dashed black curve is the sum including the X-ray line emission. As in Fig. 2, a normalization factor of 0.95 (0.2) has been applied to the hadronic (leptonic) model.

and WO stars show much larger overabundances of O and Ne, which produce the strongest lines in the spectra, so the lines would be strongly enhanced. In WN stars, carbon and oxygen have been converted to nitrogen. The O lines would be weakened, and the N VII line at 500 eV would be luminous but badly attenuated. The Ne IX and X lines at 922 and 1022 eV would then be the strongest in the spectrum at 0.5 to 1 times the strengths predicted. Thus, even in the case of a progenitor wind with anomalous abundances, we would still expect to see strong line emission in the swept-up CSM, and this would be present in the *Suzaku* observations.

4. DISCUSSION AND CONCLUSIONS

While several authors have proposed that emission lines could be undetectable in J1713 because of low shock temperatures or time-dependent ionization (e.g., Drury et al. 2009; Morlino, Amato & Blasi 2009; Berezhko & Voelk 2009), we find that a SNR with properties typically ascribed to J1713, expanding in a uniform CSM with solar elemental abundances, will produce strong X-ray emission lines when electron equilibration and non-equilibrium ionization are taken into account. This places constraints on the CSM density, n_p , and on

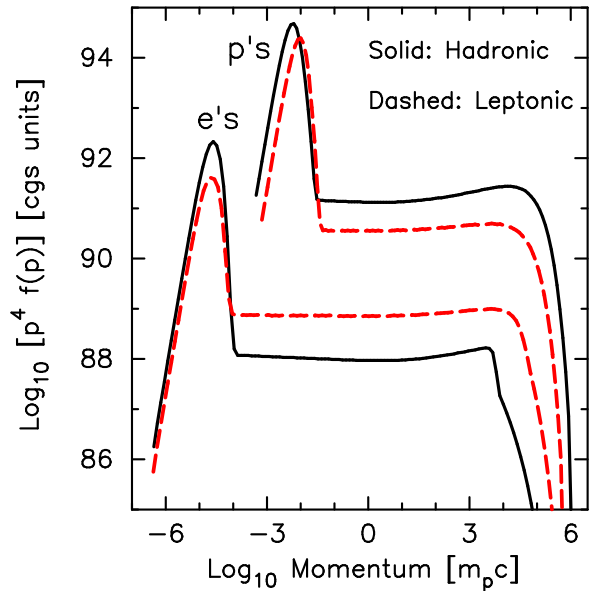


FIG. 5.— Phase-space distribution functions multiplied by p^4 for our hadronic (black solid curves) and leptonic (red dashed curves) models. These are integrated spectra at the end of the simulation in cgs units and represent the total material swept-up by the FS.

the relativistic electron to proton ratio, K_{ep} , to be consistent with *Suzaku* observations which show a smooth X-ray synchrotron continuum with no lines.

While particular values of n_p and K_{ep} will depend somewhat on details of various DSA and SNR models, in any uniform CSM model the CSM must have a relatively low density and the electron to proton ratio of shock accelerated particles must be relatively high in order to produce a satisfactory fit to the *Suzaku* data. Models where pion-decay produces the observed TeV emission require densities that are too high and values of K_{ep} that are too low to be consistent with the *Suzaku* observations. We note that we have actually only computed a lower limit to the line emission since we have not included line emission from the ejecta material heated by the reverse shock. If emission from a RS had been included, our conclusion that pion-decay is excluded could only be strengthened.

Apart from minor differences, our fit to the broad-band spectrum (bottom panel Fig. 4) is consistent with others (e.g., Porter, Moskalenko & Strong 2006; Morlino, Amato & Blasi 2009) where IC dominated the TeV emission. Our results differ substantially from the conjecture made by Drury et al. (2009) that the post-shock temperature can be reduced below X-ray emitting temperatures in strong shocks. The conclusions of Drury et al. (2009) are based on scaling arguments in the limit of extremely high sonic and Alfvén Mach numbers where the acceleration efficiency approaches 100%. In this case, the subshock may become weak enough to limit heating to the values Drury et al. (2009) suggest. However, Mach numbers as high as assumed in the Drury et al. (2009) scalings are not obtained for reasonable ambient magnetic fields and other parameters normally assigned to RX J1713.7-3946. When nonlinear effects are fully taken into account for J1713 parameters (see also, Morlino, Amato & Blasi 2009), and for acceleration efficiencies even modestly below 100%, the post-shock plasma (i.e., the proton component) is heated more

strongly than Drury et al. (2009) suggest.

We further emphasize that there is little freedom to reduce the thermal emission since we have calculated the NEI for the two electron heating extremes: Coulomb collisions and instant equilibration. For both extremes, and all cases in between, the shock heated plasma produces strong line emission. As Fig. 1 shows, it is not necessary for electrons to equilibrate with protons to become hot enough for line emission. For Coulomb collisions in our hadronic model, T_e/T_p remains less than about 0.1 for > 1600 yr.

Once it becomes clear that X-ray emission lines will be produced efficiently with a luminosity approximately $\propto n_p^2$, the intensities, I , of all the emission processes can be roughly scaled with the important parameters, n_p , K_{ep} , and the average downstream field \overline{B}_2 as:

$$I_{\text{IC}} \propto n_e^{\text{rel}} \propto n_p^{\text{rel}} K_{\text{ep}} ; \quad (1)$$

$$I_{\text{syn}} \propto n_e^{\text{rel}} \overline{B}_2^\alpha \propto n_p^{\text{rel}} K_{\text{ep}} \overline{B}_2^\alpha ; \quad (2)$$

$$I_{\text{line}} \propto I_{\text{brem}} \propto n_p^2 ; \quad (3)$$

and

$$I_{\text{pp}} \propto n_p^{\text{rel}} n_p \propto F_{\text{acc}} n_p^2 . \quad (4)$$

Here, the superscript “rel” indicates the number density of relativistic particles capable of producing the observed radiation. The factor F_{acc} is some function of the DSA efficiency, i.e., the fraction of ambient protons turned into relativistic protons capable of producing GeV-TeV emission ($n_p^{\text{rel}} \propto F_{\text{acc}} n_p$). We also assume that the relativistic protons producing pion-decay are drawn from the same population as the target protons. The expression for I_{syn} assumes the underlying electron spectrum is a power law, $dN/dE \propto E^{-\sigma}$, with $\sigma = 2\alpha - 1$.

If the TeV emission is from pion-decay, then the ratio $I_{\text{syn}}/I_{\text{pp}}$ is fixed by the observations and

$$I_{\text{syn}}/I_{\text{pp}} \propto K_{\text{ep}} \overline{B}_2^\alpha / n_p \equiv G , \quad (5)$$

where G is some constant determined by either the radio or X-ray synchrotron observations. If G is set by radio observations, radiation losses don't play a role. To hide the X-ray lines, we need to increase

$$I_{\text{syn}}/I_{\text{line}} \propto n_p^{\text{rel}} K_{\text{ep}} \overline{B}_2^\alpha / n_p^2 = n_p^{\text{rel}} G / n_p \propto F_{\text{acc}} G . \quad (6)$$

Thus, the only parameter that can change the relative intensity $I_{\text{syn}}/I_{\text{line}}$ is the DSA efficiency. The X-ray line to synchrotron continuum ratio can be changed by changing the magnetic field, but the absolute ratio of X-ray lines to gamma rays is basically fixed in the hadronic scenario. From equations 3 and 4,

$$I_{\text{line}}/I_{\text{pp}} \propto 1/F_{\text{acc}} , \quad (7)$$

and for the hadronic model (top panel in Fig. 4), $I_{\text{line}}/I_{\text{pp}}$ is more than an order of magnitude too large compared to observations to be accommodated. Changing F_{acc} and/or B cannot hide the lines if n_p is too large.

Of course, the situation is more complicated for several reasons. (1) The line emission depends importantly on the SNR evolution (i.e., the ionization age; Fig. 1) and the CSM composition. (2) The factor F_{acc} depends on the shock dynamics, the magnetic field, and uncertain

details of NL DSA. Furthermore, since radiation losses are important for relativistic electrons but not relativistic protons, $n_e^{\text{rel}}/n_p^{\text{rel}} \neq K_{\text{ep}}$ at high energies and K_{ep} depends on B for X-ray synchrotron emission. This will change the $I_{\text{syn}}/I_{\text{line}}$ scaling at X-ray energies but will not change the relative intensities of radio vs. pion-decay emission. (3) The detailed fits to the *Suzaku*, *Fermi-LAT*, and HESS data depend critically on the *shape* of the underlying electron and proton spectra in the turnover region, and on the SNR magnetic field morphology. Despite these complications, Eqs. (6) and (7), must largely control the overall scaling.

For our hadronic model shown in Figs. 2 and 4, we have chosen particular values of n_p , K_{ep} , and B_{amp} to match the shape and relative normalization of the radio, X-ray, and TeV observations. For the acceleration efficiency, we have used $\mathcal{E}_{\text{DSA}} = 0.5$, i.e., 50% of the instantaneous FS ram kinetic energy flux is put into relativistic protons. While there is little indication that larger values of \mathcal{E}_{DSA} occur in SNRs, we have explored $\mathcal{E}_{\text{DSA}} > 0.7$ and find a poorer match to the broadband observations and no improvement in the hadronic fit to the X-ray lines. One reason for this is that, in nonlinear DSA, an increase in acceleration efficiency must be accompanied by an increase in the overall shock compression ratio, R_{tot} . This translates to an increase in the downstream plasma density, a decrease in the electron temperature equilibration time, and stronger X-ray line production. Furthermore, increasing the acceleration efficiency also increases \overline{B}_2 due to compression and possibly more by MFA. Because of changes in \overline{B}_2 , increases in \mathcal{E}_{DSA} are constrained by equation 5.

On the other hand, it is easy to show that lowering \mathcal{E}_{DSA} below 0.1 is also inconsistent with the broad-band observations.

We emphasize again that the modeled shape of the turnover is both critical and uncertain. For IC and synchrotron, the shape depends on the competition between acceleration and radiation loss timescales in the acceleration region. The turnover will be further modified by radiation losses as the electrons evolve behind the shock and by diffusion of the high-energy electrons into regions of different density and magnetic field. In fact, high-energy electrons might diffuse away from regions of high magnetic field, reducing their synchrotron emission while they still emit IC. For pion-decay, the turnover depends on the maximum energy the FS can produce which depends on the self-generated diffusion of the highest energy, escaping particles.

Since these effects are yet to be described precisely, all existing SNR models, including ours, make arbitrary approximations that importantly influence the turnover shape. The fit to the shape of the *Fermi-LAT* and HESS observations is determined largely by f_{sk} , α_{cut} , and B_{amp} . The detailed fit to the shape of the *Suzaku* observations depends largely on α_{cut} and B_{amp} .

Other effects may be important as well. The synchrotron spectrum might be hardened in the turnover region by stochastic effects, as described in Bykov, Uvarov, & Ellison (2008). Furthermore, as suggested by several authors (e.g., Porter, Moskalenko & Strong 2006), a photon source in addition to the cosmic microwave background might

modify the IC fit to the high energy HESS observations.

In contrast to the shapes of the radiation spectra near their maximum energies, the relative normalizations of synchrotron, IC, pion-decay, and thermal X-ray emission are less uncertain because they depend more concretely on basic parameters. We believe that none of the approximations in our CR-hydro-NEI model are significant enough to change our basic conclusion: the constraints on ambient density and K_{ep} from thermal X-ray emission rule out pion-decay as the mechanism producing TeV emission in models with a uniform CSM.

The fact that electrons are likely producing the highest energy photons observed from RX J1713.7-3946, does not lead us to suggest that protons are absent or less energetic. Our leptonic model assumes that at any instant 25% of the shock ram kinetic energy flux goes into relativistic protons while less than 1% goes into relativistic electrons. Electrons are observed simply because they radiate more efficiently than protons in low density media. As Fig. 5 shows, the maximum proton energy is similar in our two models, i.e., $E_p^{\text{max}} \simeq 10^{14}$ eV. The increase in E_p^{max} from the higher shocked magnetic field in the hadronic model (e.g., $B_2 \simeq 36 \mu\text{G}$ at the end of the simulation vs. $B_2 \simeq 10 \mu\text{G}$ for the leptonic model) is partially offset by the smaller f_{sk} factor ($f_{\text{sk}} = 0.05$ for the hadronic model while $f_{\text{sk}} = 0.1$ for the leptonic model). The electron maximum energy is about a factor of 10 higher in the leptonic model, and the shapes of the electron spectra are different, due to the effects of radiation losses.

One result of our leptonic model, which integrates emission over the entire remnant, that may conflict with observations is the low shocked magnetic field. A low B_2 favors the leptonic model and we obtain $B_2 \simeq 10 \mu\text{G}$ for the parameters used here. Much higher estimates for B_2 have been obtained for thin X-ray filaments where the sharp X-ray edges and/or rapid time variations are attributed to strong synchrotron losses (e.g., Uchiyama et al. 2007). Our uniform CSM assumption

cannot describe filaments and it is possible that more complicated, multi-component models could account for this. For example, if the synchrotron emission originates from a smaller region than the IC emission (due, for example, to a strong but compact postshock magnetic field), then a larger field strength would be possible for a given inverse-Compton flux.

We have been careful to emphasize that we only consider a uniform CSM in this paper. While pion-decay is eliminated in this simplest case, SNR RX J1713.7-3946 is certainly more complex. As *Fermi-LAT* observations improve with time, the shape of the combined *Fermi-LAT* and HESS observations may indicate that the GeV-TeV emission is, in fact, hadronic in origin. This will require some multi-component model where relativistic protons interact with a high density target but care must still be taken to avoid inconsistency with the *Suzaku* observations. If the FS runs into a high density shell, strong X-ray lines are likely to be produced along with the enhanced pion-decay emission. If the highest energy protons escape upstream from the FS and impact a high density medium before the material is shock heated, pion-decay emission may be strong without strong accompanying X-ray line emission.

We thank Matthew Baring, Roger Blandford, Andrei Bykov, Stefan Funk, and Andrey Vladimirov for helpful discussions on this work. We thank Yasunobu Uchiyama for furnishing the *Suzaku* data. D.C.E. acknowledges support from NASA grants ATP02-0042-0006, NNH04Zss001N-LTSA, and 06-ATP06-21. P.O.S. and D.J.P. acknowledge support from NASA Contract NAS8-03060. P.O.S. and D.C.E. acknowledge support from NASA Grant NNX09AT68G. The authors are grateful to the KITP in Santa Barbara where part of this work was done when the authors were participating in a KITP program. D.C.E. also thanks KIPAC and D.J.P. acknowledges travel support from a SI Endowment Grant.

REFERENCES

- Acero, F. et al. 2009, *A&A*, 505, 157
 Aharonian, F. et al. 2006, *A&A*, 449, 223
 Amato, E. & Blasi, P. 2006, *MNRAS*, 371, 1251
 Berezhki, E. G. & Ellison, D. C. 1999, *ApJ*, 526, 385
 Berezhko, E. G. & Völk, H. J. 2008, *A&A*, 492, 995
 Berezhko, E. G. & Völk, H. J. 2009, preprint, ArXiv 0910.2094
 Blasi, P., Gabici, S. & Vannoni, G. 2005, *MNRAS*, 361, 907
 Bykov, A. M., Uvarov, Y. A. & Ellison, D. C. 2008, *ApJ*, 689, L133
 Caprioli, D., Blasi, P., Amato, E. & Vietri, M. 2008, *ApJ*, 679, L139
 Chiosi, C., & Maeder, A. 1986, *ARA&A*, 24, 329
 Crowther, P. A. 2007, *ARA&A*, 45, 177
 Drury, L. O., Aharonian, F.A., Malyshev, D. & Gabici, S. 2009, *A&A*, 496, 1
 Ellison, D. C. & Cassam-Chenaï, G. 2005, *ApJ*, 632, 920
 Ellison, D. C., Decourchelle, A. & Ballet, J. 2004, *A&A*, 413, 189
 Ellison, D.C., Moebius, E. & Paschmann, G. 1990, *ApJ*, 352, 376
 Ellison, D. C., Patnaude, D. J., Slane, P., Blasi, P. & Gabici, S. 2007, *ApJ*, 661, 879
 Funk, S. et al. 2009, Presentation *Fermi Symposium 2009* on behalf of LAT collaboration, Washington, DC
 Ghavamian, P., Laming, J. M. & Rakowski, C. E. 2007, *ApJ*, 654, L69
 Helder, E. A. et al. 2009, *Science*, 325, 719
 Kudritzki, R.-P., & Puls, J. 2000, *ARA&A*, 38, 613
 Morlino, G., Amato, E. & Blasi, P. 2009, *MNRAS*, 392, 240
 Patnaude, D. J., Ellison, D. C. & Slane, P. 2009, *ApJ*, 696, 1956.
 Porter, T. A., Moskalenko, I. V. & Strong, A. W., 2006, *ApJ*, 648, L29
 Raymond, J. C., & Smith, B. W. 1977, *ApJS*, 35, 419
 Tanaka, T. et al. 2008, *ApJ*, 685, 988
 Uchiyama, Y. et al. 2007, *Nature*, 449, 576
 Vladimirov, A. E., Bykov, A. M. & Ellison, D. C. 2009, *ApJ*, 703, L29
 Vladimirov, A., Ellison, D. C. & Bykov, A. 2006, *ApJ*, 652, 1246
 Völk, H. J., Berezhko, E. G., & Ksenofontov, L. T., 2003, *A&A*, 409, 563
 Warren, J. S., Hughes, J. P., Badenes, C., Ghavamian, P., McKee, C. F., Moffett, D., Plucinsky, P. P., Rakowski, C., Reynoso, E., & Slane, P., 2005, *ApJ*, 634, 376
 Weaver, R., McCray, R., Castor, J., Shapiro, P., & Moore, R. 1977, *ApJ*, 218, 377
 Williams, B.J. et al. 2009, *ApJ*, 652, L33
 Zirakashvili, V. N. & Aharonian, F.A. et al. 2009, preprint arXiv0909.2285